Correlation-Enhanced Effective Mass of Two-Dimensional Electrons in $Mg_xZn_{1-x}O/ZnO$ Heterostructures

Y. Kasahara,[1,*] Y. Oshima,[2] J. Falson,[1] Y. Kozuka,[1] A. Tsukazaki,[1,3] M. Kawasaki,[1,4] and Y. Iwasa[1,4]

[1]*Quantum-Phase Electronics Center (QPEC) and Department of Applied Physics, University of Tokyo, Tokyo 113-8656, Japan*

[2]*RIKEN, Wako, Saitama 351-0198, Japan*

[3]*Department of Advanced Materials Science, University of Tokyo, Kashiwa, Chiba 277-8561, Japan*

[4]*Correlated Electron Research Group (CERG), RIKEN-ASI, Wako 351-0198, Japan*

(Received 24 September 2012; published 10 December 2012)

We performed combined magnetotransport and cyclotron resonance experiments on two-dimensional electron systems confined in the $Mg_xZn_{1-x}O/ZnO$ heterostructures over a wide range of carrier densities, from 1.9 to 12×10^{11} cm^{-2} ($3.5 \lesssim r_s \lesssim 10$, where r_s is the Wigner-Seitz radius). As the carrier density was reduced, the transport mass m^*_{tr} was strongly enhanced. In marked contrast, the effective masses determined from the cyclotron resonance m^*_{CR} were found to be independent of the carrier density and as large as the bulk effective mass. The large enhancement of m^*_{tr}, which exceeds m^*_{CR} by ~60%, at the lowest carrier density with $r_s \sim 10$ is purely attributed to the strong electron correlation.

DOI: 10.1103/PhysRevLett.109.246401 PACS numbers: 71.18.+y, 73.43.Qt, 76.40.+b

Oxide heterostructures have been successful in demonstrating novel electronic states at their interfaces [1], where the physical phenomena observed are expected to be dominated by electron correlation effects. A prerequisite to the clear observation of such phenomena resides in improving growth techniques, in order to provide the very clean two-dimensional electron systems (2DESs). Recently, the $Mg_xZn_{1-x}O/ZnO$ heterostructure has emerged as an ideal system for investigating the correlation effects in 2DESs at oxide interfaces, where extremely clean 2DESs have exhibited the quantum Hall effect [2,3] and mobilities as high as 800 000 cm^2/V s [4,5]. Compared to the widely studied AlGaAs/GaAs system, the smaller dielectric constant ($\varepsilon = 8.5$) and larger bulk effective mass of $m^*_{bulk} = 0.29m_0$ (m_0 is the bare electron mass) in ZnO strengthen the correlation effects, which are characterized by the Wigner-Seitz radius $r_s = 1/\sqrt{\pi n}a^*_B$, where n is the carrier density and a^*_B is the effective Bohr radius $[(\varepsilon/\varepsilon_0)/(m^*_{bulk}/m_0)]a_B$ (ε_0 is the vacuum permittivity and a_B is the Bohr radius). In the low carrier-density regime, where $r_s \gg 1$, transport measurements in high magnetic fields have indicated the presence of strong electron correlation in the 2DESs in $Mg_xZn_{1-x}O/ZnO$ through the observations of enhanced effective electron masses and spin susceptibilities [4,6]. However, other experimental probes, presumably optical techniques, are requisite for quantitative discussion and understanding of the correlation effects.

Cyclotron resonance (CR) is a powerful probe to determine the effective electron masses. For a translationally invariant isotropic electron gas, a long wavelength radiation can couple only to the center of mass of electron motion, which is not affected by the electron-electron interactions, giving the effective mass m^*_{CR} renormalized only by the electron-phonon interactions (Kohn's theorem [7]). On the other hand, the transport mass m^*_{tr} is additionally influenced by the electron-electron interactions due to the presence of the quasiparticle drag. Therefore, a comparison between m^*_{CR} and m^*_{tr} can be a unique tool of gauging the magnitude of the correlation effects. We wish to point out, however, that the theorem for CR can be violated especially for multiband systems [8,9]. The 2DESs in the $Mg_xZn_{1-x}O/ZnO$ heterostructures offer an ideal platform for the comparative study, since the electrons in this novel structure occupy an isotropic single pocket with a large band mass in contrast with the other 2DESs having complex band structures and/or light electron masses.

Here, we report combined magnetotransport and CR experiments on 2DESs confined in the $Mg_xZn_{1-x}O/ZnO$ heterostructures. CR measurements of $Mg_xZn_{1-x}O/ZnO$ have previously been reported for a dense 2DES with $n \sim 6 \times 10^{12}$ cm^{-2} ($r_s \sim 1.5$) where the correlation effects are expected to be less pronounced [10]. In this study, we investigated dilute 2DESs in $Mg_xZn_{1-x}O/ZnO$ with significantly higher r_s ($3 \lesssim r_s \lesssim 10$) and observed clear discrepancies in the measured effective masses in the low carrier-density regime. The effective mass determined from the CR measurements was independent of the sheet carrier density, and its magnitude was comparable to the bulk effective mass. These results are in contrast to those of magnetotransport measurements, in which a strong enhancement of the effective mass was observed at carrier densities below 5×10^{11} cm^{-2}. These results provide direct evidence that the electron-electron interactions play a significant role in the mass enhancement of two-dimensional electrons in $Mg_xZn_{1-x}O/ZnO$.

The $Mg_xZn_{1-x}O/ZnO$ heterostructures were grown by molecular beam epitaxy utilizing distilled pure ozone as described in Ref. [5]. In this study, we prepared three samples with different sheet carrier densities n_{2D} and mobilities μ [inset in Fig. 1(a)], which are controlled by

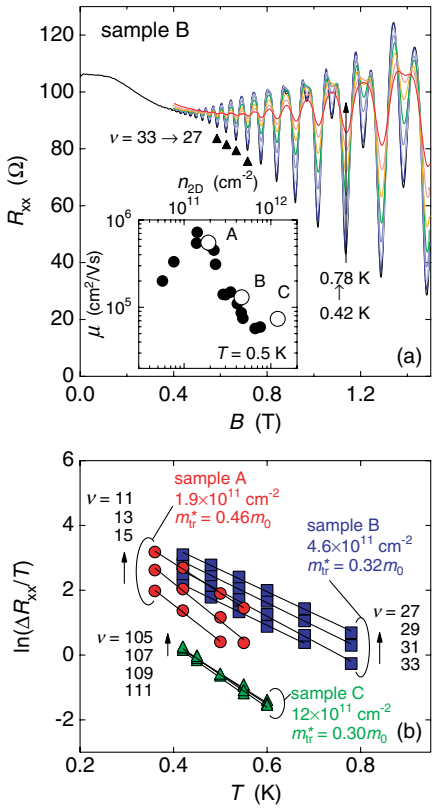

FIG. 1 (color online). (a) Temperature dependence of the SdH oscillations from 0.36 to 0.78 K for sample B. Triangles indicate the Landau filling factor ν used to evaluate the transport mass m^*_{tr}. The inset shows the mobility μ as a function of the sheet carrier density n_{2D} of the samples (open circles) with data from Ref. [5] (filled circles). (b) Temperature dependence of $\ln(\Delta R_{xx}/T)$, where ΔR_{xx} denotes the amplitude of SdH oscillations, for the samples used in the present study. The solid lines represent the fits to the data for estimating m^*_{tr}.

Mg content in the barrier layer of $Mg_xZn_{1-x}O/ZnO$ heterostructure [5]. Sample A is identical to a sample utilized in Ref. [4]. n_{2D} and μ were determined from the Hall effect and Shubnikov–de Haas (SdH) oscillations at 0.5 K, along with the zero field resistance. The CR measurements were performed in the frequency range from 9 to 400 GHz by using the same batch of samples that were used in the magnetotransport measurements. The typical lateral dimension of the samples for the CR measurements is 1×2 mm^2. At the lowest frequency of 9.1 GHz, we investigated CR by using a standard X-band microwave spectrometer (JASCO, FA-300) with a cylindrical TE_{011} cavity [11,12]. The samples were placed as close as possible to the nodal plane of the electric microwave field where the magnetic field is maximized. Coupling to the cyclotron and plasmon modes can occur due to inevitable microwave electric field due to the finite sample size and fringe fields in the perturbed cavity [11,12]. The static magnetic field is modulated at a frequency of 10 kHz and an amplitude of 20 mT. The microwave response was obtained as the first derivative of the cavity transmission spectrum with respect to the magnetic field. The temperature was lowered down to 6 K by using a continuous helium flow cryostat. The CR measurements above 30 GHz were performed by using a cavity perturbation technique from 30 to 100 GHz and using a transmission method with a Fabry-Perot resonator from 100 to 400 GHz. A direct transmission spectrum was obtained in the frequency range above 30 GHz with a sweeping magnetic field which is generated by a superconducting magnet up to 7 T. The temperature was controlled by using a variable temperature insert equipped in a liquid helium dewar.

First, the transport mass m^*_{tr} was determined through a Dingle analysis of the temperature dependence of the SdH oscillations. The oscillations in the longitudinal resistance R_{xx} were recorded over the temperature range from 0.3 to 0.9 K. Figure 1(a) shows the temperature dependence of the SdH oscillations of sample B. The applied magnetic field was perpendicular to the sample plane. Figure 1(b) depicts the temperature dependence of $\ln(\Delta R_{xx}/T)$, where ΔR_{xx} is the amplitude of the SdH oscillations at fixed magnetic field. ΔR_{xx} was analyzed by using the Dingle expression $\Delta R_{xx} \propto \exp(-\pi/\omega_c\tau_q)\chi/\sinh\chi$, where $\chi = 2\pi^2 k_B T/\hbar\omega_c$ (k_B is the Boltzmann constant), $\omega_c = eB/m^*_{tr}$ is the cyclotron frequency, and τ_q is the quantum scattering time. Assuming that τ_q is temperature-independent over the temperature range of the measurements, we determined m^*_{tr} from fits to the $\ln(\Delta R_{xx}/T)$ vs T plots. The obtained m^*_{tr} increases with decreasing carrier density.

We now move onto the CR analysis of the heterostructure. Figure 2 shows the first derivative of the 9.1 GHz cavity transmission spectra with respect to the magnetic field at 6 K in the $Mg_xZn_{1-x}O/ZnO$ heterostructures. The static magnetic field B was applied perpendicular to the sample plane [$\theta = 0°$, where θ is the angle between the magnetic field and the direction normal to the sample plane (left inset in Fig. 2)]. Both the electron spin resonance and the CR from the 2DES can be observed in this 9.1 GHz cavity experiment [11]. The observed spectra exhibited broad signals with large amplitudes, clearly indicating that CR is dominant. In the right inset in Fig. 2, the spectrum for sample C, measured at various magnetic field orientations, is shown as a function of the perpendicular component of the applied magnetic field $B\cos\theta$. The position of the peak scales with $B\cos\theta$, providing direct evidence that the signal arises from two-dimensional electrons [12]. However, the electron spin resonance signal from the 2DES was not observed in this study, possibly due to the limited experimental resolution.

The line shape and resonance position of the spectrum varied significantly among the samples. However, in all samples, the observed resonance fields were shifted toward higher magnetic fields, from 0.4 to 0.6 T, with respect to the expected pure CR at 0.1 T for the bulk effective mass of ZnO. This shift may originate from a coupling between the

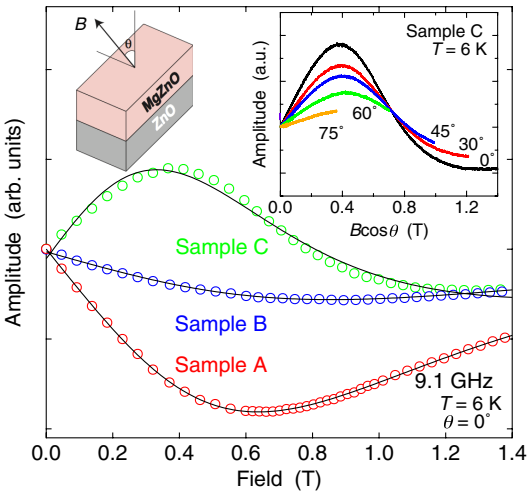

FIG. 2 (color online). The first derivative of the 9.1 GHz cavity transmission spectra measured at 6 K. The static magnetic field was applied normal to the surface of the heterostructures ($\theta = 0°$). The solid lines represent the least-squares fits using a model of magnetoplasmon resonance and the Drude model of momentum relaxation [12]. The left inset presents the configuration of the measurement. The right inset shows the spectra for sample C as a function of the perpendicular component of the applied magnetic field, $B\cos\theta$.

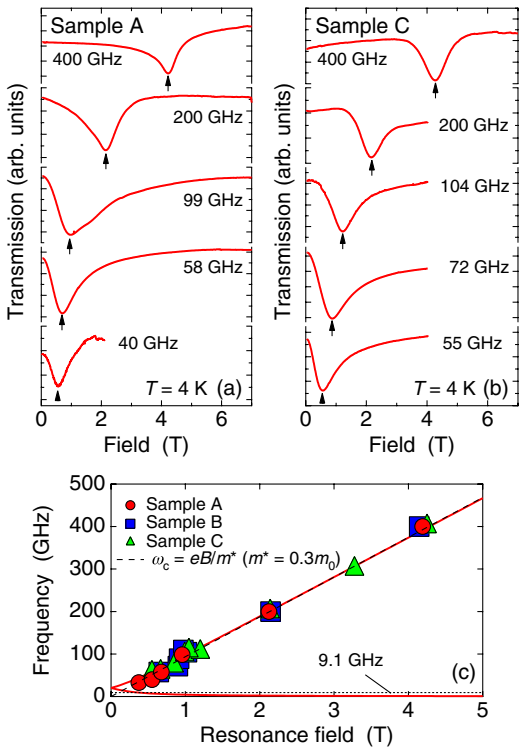

FIG. 3 (color online). Typical transmission spectrum as a function of the magnetic field for various excitation frequencies at 4 K for (a) sample A and (b) sample C. Spectra below 100 GHz were taken by using a cavity perturbation technique, and those above 100 GHz were taken by using a transmission method. The arrows indicate the resonance fields. (c) Frequency as a function of the resonance fields. The dotted line indicates the frequency used by the X-band microwave spectrometer, 9.1 GHz. The dashed line is a linear fit and indicates an effective mass of $0.30m_0$ using the conventional relationship between cyclotron frequency and effective mass, $\omega_c = eB/m^*$. The solid lines represent the calculated resonance frequency with $m^* = 0.30m_0$ and a plasma frequency of $\omega_p/2\pi = 20$ GHz.

cyclotron motion and the plasma oscillations. It has been observed for several 2DESs in heterostructures that the cyclotron motion and plasma oscillations will hybridize when the frequencies of the two modes approach each other (coupled plasmon-cyclotron or magnetoplasmon modes) [12–14]. The resonance frequency splits into the upper cyclotronlike branch and the lower edge magnetoplasmon mode, and these frequencies are given by $\omega_{\rm res}^{\pm} = \pm\frac{\omega_c}{2} + \sqrt{\omega_p^2 + (\omega_c/2)^2}$, where $\omega_p = \sqrt{n_{2D}e^2/[m^*(1+\varepsilon)\varepsilon_0 R]}$ (R is the radius of a disk-shaped sample) is the plasma frequency. In the present samples, $\omega_p/2\pi$ was estimated to be approximately 20 GHz for sample C, indicating that the spectra shown in Fig. 2 are dominated by the edge magnetoplasmon mode. The observed spectrum can be fitted by a model considering the Drude model of momentum relaxation with respect to the cyclotron-active ($\omega_{\rm res}^{+}$) and cyclotron-inactive ($\omega_{\rm res}^{-}$) contributions to the magnetoplasmon resonance (solid lines in Fig. 2) [12]. The observation of the edge magnetoplasmon resonance confirms the presence of high-quality two-dimensional electrons and indicates that CR measurements far above 20 GHz are required to determine the effective electron mass in the 2DESs of $Mg_xZn_{1-x}O/ZnO$ heterostructures.

Figures 3(a) and 3(b) show typical transmission spectra measured above 30 GHz for sample A and C, respectively. The external magnetic field was applied perpendicular to the plane ($\theta = 0°$). A broad but distinct resonance was observed as a dip in the entire frequency range. The temperature dependence measurements revealed no significant change in the resonance position at least below 10 K within the experimental error (not shown). The resonance field shifts to higher fields with increasing excitation frequency, indicating that the resonances are attributed to the CRs originating from 2DESs. Figure 3(c) displays the excitation frequency as a function of the resonance fields. The resonance fields of the samples coincide with each other. At higher fields, the data follow a nearly straight line with an intersect at 0 T (shown by the dashed line), and an effective mass of $(0.30 \pm 0.05)m_0$ can be derived by using the conventional relationship between the mass and the cyclotron frequency. The resonance frequency $\omega_{\rm res}^{\pm}$, which was calculated by using $\omega_p/2\pi \simeq 20$ GHz and the effective mass of $0.30m_0$ [solid lines in Fig. 3(c)], exhibits good agreement with the experimental results.

Figure 4 displays the n_{2D} dependence of the effective masses in the 2DESs of Mg_xZn_{1-x}/ZnO heterostructures,

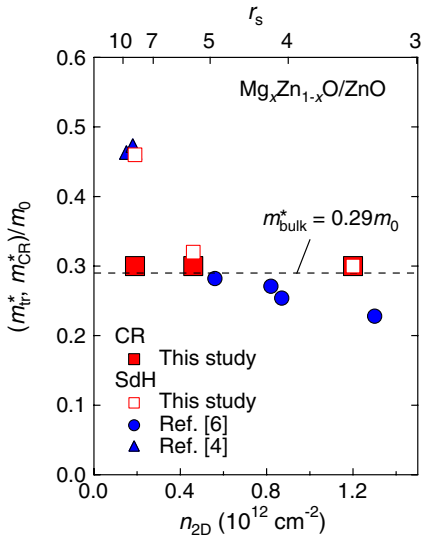

FIG. 4 (color online). The effective electron masses, which are obtained by the CR and SdH oscillations, as a function of the sheet carrier density. The dashed line indicates the bulk effective mass of ZnO m^*_{bulk}.

obtained by the present magnetotransport and CR measurements, m^*_{tr} (open squares) and m^*_{CR} (filled squares), respectively. Values of m^*_{tr} obtained in previous reports [4,6] are also plotted (circles and triangles). With reducing n_{2D}, m^*_{tr} is steeply enhanced when $r_s > 5$ and exceeds m^*_{bulk} by ~60% when $r_s \sim 10$. Similar mass enhancements at low carrier densities have been observed in several 2DESs such as AlGaAs/GaAs [15], AlGaAs/AlAs [16], and Si-based metal-oxide-semiconductor field-effect transistors [17]. In contrast, m^*_{CR} is nearly independent of the carrier density.

Here, we discuss the mass renormalization effects of the SdH oscillations and CR. Because of the single-valley nature of the present 2DESs of Mg_xZn_{1-x}/ZnO heterostructures, effective masses can be simply estimated as $m^*_{CR} = (1 + \lambda_{e-p})m_{band}$ and $m^*_{tr} = (1 + \lambda_{e-p})(1 + \lambda_{e-e})m_{band}$, where λ_{e-p} and λ_{e-e} are the $e - p$ and $e - e$ coupling constants, respectively, and m_{band} is the bare band mass. We found that, by using $m_{band} = 0.24m_0$ [18], $\lambda_{e-p} = 0.25$ and λ_{e-e} increases from 0 to 0.53 with decreasing n_{2D}. The observed $m^*_{CR} = 0.30m_0$ is very close to the polaron effective mass of $0.29m_0$ in the bulk ZnO [18] and is consistent within experimental error with the value previously reported ($0.32m_0$) at the higher carrier density [10]. In ideal 2DESs, the polaron mass correction becomes larger than the bulk [19], but observed m^*_{CR} was always smaller than the ideal correction. However, the mass correction may be reduced by several possible effects, including screening and subband effects [20], and reduced polaron mass corrections have been demonstrated in several heterostructures [21].

Our results provide strong evidence that the observed enhancement of m^*_{tr} compared to m^*_{CR} at the lowest carrier density originates purely from electron-electron interactions, giving rise to an r_s as high as 10, which is difficult to achieve in other semiconductors. m^*_{tr}/m^*_{CR}, which gauges the strength of the correlation effects, at the lowest n_{2D} in Mg_xZn_{1-x}/ZnO is comparable to that of GaAs-based single-valley 2DESs [15,22]. Accessing the low carrier-density limit of $n_{2D} < 1 \times 10^{11}$ cm^{-2}, which would further increase the correlation effects, while maintaining a large transport scattering time is challenging. A metal-insulator transition is expected to be realized at $r_s > 35$ at zero field [23], but it has been suggested that this transition may occur at a lower r_s value in magnetic fields [24], which makes the ZnO heterostructures ideal systems for investigating unexplored quantum phases of two-dimensional carriers.

In conclusion, we have reported the magnetotransport and cyclotron resonance measurements on the two-dimensional electron systems confined in the $Mg_xZn_{1-x}O/ZnO$ heterostructures over a wide range of carrier densities. The effective masses determined from the cyclotron resonance are independent of the carrier density and as large as the bulk effective mass. The observed significant enhancement of m^*_{tr} compared to m^*_{CR} at the lowest carrier density ($r_s \sim 10$) is a direct consequence of the strong electron correlation.

We thank R. Kato for his experimental support in the cyclotron resonance measurements. This work was supported in part by a Grant-in-Aid for Scientific Research (S) (Grant No. 21224009) and for Young Scientists (B) (Grant No. 2474022), the "Funding Program for World-Leading Innovative R&D on Science and Technology (FIRST Program)" from JSPS, and the Strategic International Collaborative Research Program (SICORP) from JST, Japan. The measurements that used an X-band spectrometer were conducted in Research Hub for Advanced Nano Characterization, The University of Tokyo, supported by MEXT, Japan. Y. K. was partly supported by Murata Science Foundation. A. T. was partly supported by a Grant-in-Aid for Young Scientists (A) (Grant No. 23686008) from JSPS, Japan.

*kasahara@ap.t.u-tokyo.ac.jp

[1] H. Y. Hwang, Y. Iwasa, M. Kawasaki, B. Keimer, N. Nagaosa, and Y. Tokura, Nat. Mater. **11**, 103 (2012).
[2] A. Tsukazaki, A. Ohtomo, T. Kita, Y. Ohno, H. Ohno, and M. Kawasaki, Science **315**, 1388 (2007).
[3] A. Tsukazaki, S. Akasaka, K. Nakahara, Y. Ohno, H. Ohno, D. Maryenko, A. Ohtomo, and M. Kawasaki, Nat. Mater. **9**, 889 (2010).
[4] D. Maryenko, J. Falson, Y. Kozuka, A. Tsukazaki, M. Onoda, H. Aoki, and M. Kawasaki, Phys. Rev. Lett. **108**, 186803 (2012).
[5] J. Falson, D. Maryenko, Y. Kozuka, A. Tsukazaki, and M. Kawasaki, Appl. Phys. Express **4**, 091101 (2011).
[6] A. Tsukazaki *et al.*, Phys. Rev. B **78**, 233308 (2008).
[7] W. Kohn, Phys. Rev. **123**, 1242 (1961).

[8] M. Yoshida, K. Koyama, A. Ochiai, and M. Motokawa, Phys. Rev. B **71**, 075102 (2005).
[9] M. Kimata *et al.*, Phys. Rev. Lett. **107**, 166402 (2011).
[10] Y. Imanaka, T. Takamasu, H. Tampo, H. Shibata, and S. Niki, Phys. Status Solidi C **7**, 1599 (2010).
[11] Z. Wilamowski, W. Jantsch, H. Malissa, and U. Rössler, Phys. Rev. B **66**, 195315 (2002).
[12] A. Wolos, W. Jantsch, K. Dybko, Z. Wilamowski, and C. Skierbiszewski, Phys. Rev. B **76**, 045301 (2007).
[13] S. J. Allen, Jr., H. L. Störmer, and J. C. M. Hwang, Phys. Rev. B **28**, 4875 (1983).
[14] W. Pan, K. Lai, S. P. Bayrakci, N. P. Ong, D. C. Tsui, L. N. Pfeiffer, and K. W. West, Appl. Phys. Lett. **83**, 3519 (2003).
[15] Y.-W. Tan, J. Zhu, H. L. Stormer, L. N. Pfeiffer, K. W. Baldwin, and K. W. West, Phys. Rev. Lett. **94**, 016405 (2005).
[16] M. Padmanabhan, T. Gokmen, N. C. Bishop, and M. Shayegan, Phys. Rev. Lett. **101**, 026402 (2008).
[17] V. M. Pudalov, M. E. Gershenson, H. Kojima, N. Butch, E. M. Dizhur, G. Brunthaler, A. Prinz, and G. Bauer, Phys. Rev. Lett. **88**, 196404 (2002).
[18] W. S. Baer, Phys. Rev. **154**, 785 (1967).
[19] S. D. Sarma, Phys. Rev. B **27**, 2590 (1983).
[20] M. H. Degani and O. Hipólito, Phys. Rev. B **35**, 7717 (1987).
[21] M. A. Brummell, R. J. Nicholas, M. A. Hopkins, J. J. Harris, and C. T. Foxon, Phys. Rev. Lett. **58**, 77 (1987).
[22] W. Zawadzki, C. Chaubet, D. Dur, W. Knap, and A. Raymond, Semicond. Sci. Technol. **9**, 320 (1994).
[23] B. Tanatar and D. M. Ceperley, Phys. Rev. B **39**, 5005 (1989).
[24] Y. Kozuka, A. Tsukazaki, D. Maryenko, J. Falson, S. Akasaka, K. Nakahara, S. Nakamura, S. Awaji, K. Ueno, and M. Kawasaki, Phys. Rev. B **84**, 033304 (2011).